THE EUROPEAN
PHYSICAL JOURNAL C

Electroweak corrections to the angular coefficients in finite-p_T Z-boson production and dilepton decay

Rikkert Frederix[a], Timea Vitos[b]

Theoretical Particle Physics, Department of Astronomy and Theoretical Physics, Lund University, Sölvegatan 14 A, 223 62 Lund, Sweden

Abstract We present next-to-leading order (NLO) electroweak corrections to the dominant five angular coefficients parametrizing the Drell–Yan process in the Z-boson mass peak range for finite-p_T vector boson production. The results are presented differentially in the vector boson transverse momentum. The Lam–Tung violating difference $A_0 - A_2$ is examined alongside the coefficients. A single lepton transverse momentum cut is needed in the case of electroweak corrections to avoid a double singularity in the photon induced diagrams, and the dependence on the value of this cut is examined. We compare the electroweak corrections to the angular coefficients to the NLO QCD corrections, including the single lepton cut. The size of the single lepton cut is found to affect the two coefficients A_0 and A_2 to largest extent. The relative size of the electroweak corrections to the coefficients is moderate for all single lepton cut values, and by extrapolation to the inclusive results, is moderate also for the full dilepton phase space case. However, for the Lam–Tung violation, there is a significant contribution from the electroweak corrections for low p_T of the lepton pair.

1 Introduction

With a new era of LHC runs lying ahead, accounting for Standard Model background signatures with great accuracy becomes increasingly important. Electroweak (EW) corrections are, by nature of the magnitudes of the gauge couplings in the Standard Model, at energy scales relevant to present collisions, an order smaller than the strong corrections. This implies that EW corrections are, when accuracy is difficult to obtain, not of primary interest. However, in processes where precision reaches that of predictions at next-to-next-to-leading order (NNLO) QCD, an inclusion of electroweak corrections is necessary.

[a] e-mail: rikkert.frederix@thep.lu.se

[b] e-mail: timea.vitos@thep.lu.se (corresponding author)

The Drell–Yan process of lepton pair production in hadron–hadron collisions has been of significant interest for the past years in particle physics because of its high availability in experiment and important implications for the parton model [1]. Due to the clear signatures in experiment, this process together with deep inelastic scattering, are the benchmark processes for determination of parton distribution functions. A precise theory prediction for the Drell–Yan process is of high importance for fundamental particle physics research. The related process of charged heavy vector boson production and decay, with a final state $l^\pm \nu_l$ requires similar analysis, but due to difficulties in missing energy measurements, the signature for this process is less propitious than for the neutral current process.

The lepton pair production in hadron–hadron collisions was first discussed in Ref. [2]. The Drell–Yan process was examined in the parton model, and the leading order $\mathcal{O}(\alpha^2)$ expression for the process in terms of parton distribution functions was presented. This was shortly followed by NLO QCD corrections to the process in Ref. [3], obtaining large $\mathcal{O}(\alpha^2 \alpha_S)$ corrections. During the following years, one benchmark work was that of Ref. [4] where the angular distribution of the lepton pair was investigated. In the work [5,6] the cross section in terms of structure functions for the hadronic current was studied, assuming solely a (virtual) photon interaction and introducing the Lam–Tung relation, in analogy with the Callan–Gross relation for deep inelastic scattering [7]. Dilepton production arising from both virtual photon and Z-boson decays was first covered in Ref. [8], where the first five of the angular coefficients were considered at finite-p_T vector boson production. The remaining three angular coefficients vanish at order $\mathcal{O}(\alpha^2 \alpha_S)$ and hence are not considered up to NNLO QCD.

In contrast to the zero-p_T Drell–Yan process $pp \to Z \to l^+l^-$, in this work we consider the finite-p_T Drell–Yan process $pp \to Z+X \to l^+l^- +X$, whose leading order is given by $\mathcal{O}(\alpha^2 \alpha_S)$. The kinematics of this process is parametrized

by eight angular coefficients [4], each containing information of the spin state of the vector boson. Calculation of these angular coefficients has been presented previously up to NNLO QCD in Refs. [9,10]. Two of the coefficients, A_0 and A_2 satisfy at leading order $\mathcal{O}(\alpha^2 \alpha_S)$ the Lam–Tung relation $A_0 - A_2 = 0$ [5,6], a manifestation of the spin properties of the vector boson and the leptons. Measurements of these angular coefficients have been performed previously at Tevatron [11,12], at CMS [13] and most recently at ATLAS [14]. The experimental data shows a larger violation of the Lam–Tung relation than is predicted at NNLO QCD $\mathcal{O}(\alpha^2 \alpha_S^3)$ in Ref. [10]. Efforts to describe this discrepancy have been made [15] in terms of non-perturbative effects [16] and spin asymmetries [17]. The motivation of the present work is to investigate the electroweak effects at fixed order to this process.

The outline of the article is the following. In Sect. 2, we present the theoretical setup and address electroweak corrections and how these are to be treated in the prevailing work. In Sect. 3, we discuss the numerical setup, the selection criteria, and discuss our treatment of the theoretical uncertainties. In Sect. 4 we present the results and finally discuss these in Sect. 5.

2 Theoretical setup

2.1 Angular coefficients

To introduce notation, we consider the following high energy proton-proton (pp) collisions to a dilepton final state (l^+l^-),

$$p(k_1) + p(k_2) \rightarrow l^+(k_3) + l^-(k_4) + X(k_5) \tag{1}$$

where we indicate the momentum of each particle in brackets and X has been introduced as the recoil to the lepton pair. In the region where the lepton pair invariant mass $m_{ll}^2 = (k_3 + k_4)^2$ is in the Z-boson pole range, the dominant contribution to the process is the Z-boson production and decay

$$p + p \rightarrow Z + X \rightarrow l^+ + l^- + X, \tag{2}$$

while the photon mediated process is present but subdominant due to the large virtuality of the photon. The Z-boson momentum is then given by the lepton pair momentum, $p_Z = k_3 + k_4$ with transverse momentum $p_{T,Z}$ and rapidity y_Z. The spin polarization of the vector boson directly affects the angular distribution of the lepton pair. For the zero-p_T Drell–Yan process this yields a $(1 + \cos\theta)^2$ dependence, in similarity to the W-boson production, however, at finite-p_T this simple dependence changes [18].

The differential cross section for the process can be expanded in terms of real spherical harmonics and associated coefficients which bare the dependencies on the vector boson kinematics. The angular coefficients appearing in the expansion are ratios between the different spin states and the

unpolarized cross section, and can be analytically determined at next-to-leading order in QCD [9,18]. Numerous notations exist for the decomposition of the differential cross section into structure functions or helicity amplitudes. We follow the one in Refs. [10,18], where the decomposition is into eight frame-dependent angular coefficients denoted by A_i with $i = 0, \ldots, 7$. In this work the choice of frame is the Collins–Soper frame (see below), in which case the (negatively charged) lepton angular coordinates in the frame are ϕ (azimuthal) and θ (polar). The expansion in this notation reads

$$\begin{aligned}
\frac{\mathrm{d}\sigma}{\mathrm{d}p_{T,Z}\mathrm{d}y_Z\mathrm{d}m_{ll}\mathrm{d}\Omega} &= \frac{3}{16\pi} \frac{\mathrm{d}\sigma^{U+L}}{\mathrm{d}p_{T,Z}\mathrm{d}y_Z\mathrm{d}m_{ll}} \\
&\times \Bigg((1 + \cos^2\theta) + A_0 \frac{1}{2}(1 - 3\cos^2\theta) \\
&+ A_1 \sin 2\theta \cos\phi \\
&+ A_2 \frac{1}{2} \sin^2\theta \cos 2\phi \\
&+ A_3 \sin\theta \cos\phi + A_4 \cos\theta \\
&+ A_5 \sin^2\theta \sin 2\phi + A_6 \sin 2\theta \sin\phi \\
&+ A_7 \sin\theta \sin\phi \Bigg),
\end{aligned} \tag{3}$$

where σ^{U+L} denotes the unpolarized cross section.

At leading order, the coefficients are (linear combinations of) the structure functions of the hadronic tensor $W_{\mu\nu}$ in the amplitude decomposition $\mathcal{M} \propto W_{\mu\nu}L^{\mu\nu}$ with the probing leptonic tensor $L^{\mu\nu}$. At order $\mathcal{O}(\alpha^2\alpha_S)$, the Lam–Tung relation between two of these coefficients reads

$$A_0 - A_2 = 0, \tag{4}$$

which can be derived using the properties of the amplitudes.

The real spherical harmonics $Y_{lm}(\theta, \phi)$ present in Eq. (3) are of order $l \leq 2$. Following Ref. [10], we use the orthogonality relation

$$\int Y_{lm}(\theta, \phi)Y_{l'm'}(\theta, \phi)\mathrm{d}\Omega = \delta_{ll'}\delta_{mm'} \tag{5}$$

to project out the angular coefficients $A_i(m_{ll}, p_{T,Z}, y_Z)$, using a weighted normalization

$$\langle f(\theta, \phi)\rangle = \frac{\int \mathrm{d}\Omega \mathrm{d}\sigma f(\theta, \phi)}{\int \mathrm{d}\Omega \mathrm{d}\sigma}, \tag{6}$$

with the usual solid angle differential $\mathrm{d}\Omega = \mathrm{d}\phi \mathrm{d}\cos\theta$. This can be implemented in Monte Carlo calculation by reweighting each event with the corresponding function $f(\theta, \phi)$.

A note on the chosen frame of reference: a suitable choice is a rest frame of the vector boson, in which the angular dependence of the final state leptons can be analyzed. We perform the calculations in the Collins–Soper reference frame [4], in which previous works on the angular coefficients have

been performed, and the frame adopted by LHC measurements. This frame is defined as the rest frame of the heavy vector boson in which the z-axis is chosen to be along the external bisector of the two incoming parton momenta, with the positive direction in the same direction as the lepton pair in the laboratory frame. The x-axis is chosen to be along the bisector of the incoming parton momenta, with the positive direction opposite to the sum of the two incoming parton momenta. The y-axis is then chosen to complete a right-handed Cartesian coordinate system.

2.2 NLO electroweak corrections

The NLO EW corrections to the dilepton + jet final state have been first computed by Denner et al. [19]. We classify the contributions to the perturbative structure of the cross section in Eq. (2) up to next-to-leading order in the gauge couplings in the following manner

$$d\sigma^{(\text{LO})} = \alpha^2 \alpha_S B_1, \tag{7}$$

$$d\sigma^{(\text{NLO QCD})} = \alpha^2 \alpha_S B_1 + \alpha^2 \alpha_S^2 C_1, \tag{8}$$

$$d\sigma^{(\text{NLO EW})} = \alpha^2 \alpha_S B_1 + \alpha^3 B_2 + \alpha^3 \alpha_S C_2, \tag{9}$$

where the B_i (at LO) and C_i (at NLO) label finite values obtained by evaluation of the corresponding Born and virtual and real emission diagrams, respectively. In the NLO EW term, we also include the subleading term at Born-level, $\alpha^3 B_2$. Note that the last term in Eq. (9) is to be interpreted as both electroweak $\mathcal{O}(\alpha)$ corrections to the LO term $\alpha^2 \alpha_S B_1$, but also as the QCD corrections at $\mathcal{O}(\alpha_S)$ to the term $\alpha^3 B_2$. By not including the $\alpha^3 B_2$ term at LO in Eq. (8), this term is also omitted in the NLO QCD corrections (which is consistent, as this contribution is negligible to the $\alpha^2 \alpha_S^2 C_1$ term). We consistently include the photon induced processes in order to obtain the correct IR cancellations. We obtain the cross section up to NLO QCD + EW using the additive approach,

$$d\sigma^{(\text{NLO QCD+EW})} = d\sigma^{(\text{NLO QCD})} + d\sigma^{(\text{NLO EW})}$$
$$- d\sigma^{(\text{LO})}. \tag{10}$$

For the electroweak corrections to the angular coefficients, in the presence of real photon emission from the external leptons, the expansion in Eq. (3) is a priori not valid. The three-body decay $Z \rightarrow l^+ l^- \gamma$ alters the kinematics. As a direct distinction of such a hard photon is not possible, we attempt to analyze the angular coefficients as given by this expansion and examine to what extent this expansion is valid in the case of electroweak corrections. Hence, a direct comparison to the theoretically derived angular coefficients would not be well-motivated. We perform a comparison between the QCD corrections and the QCD + EW corrections to the coefficients

as obtained by the projection Eq. (6) to qualitatively examine the effect.

3 Numerical setup

3.1 Basic cuts and parameters

For the evaluation of the differential cross sections, we use MADGRAPH5_AMC@NLO [20,21] for the process $pp \rightarrow l^+ l^- j$ at $\sqrt{s} = 8$ TeV at fixed order. We work in a five-flavor scheme, where all lepton and quark masses except for the top quark are set to zero. In order to generate the lepton pair at non-zero transverse momentum, we add the parton j to the process, which can be a (anti) quark, gluon or photon.[1]

For the input parameters, we adapt the complex-mass-scheme [23,24], in which (in our case) the masses of the heavy vector bosons and the top quark are treated as complex numbers, thus rendering the dependent parameters complex. In order to maintain correct cancellations in the subtraction schemes, we use the $\bar{G}_\mu$ scheme [21], in which the G_μ constant obtains a phase, compensating for the phase of the electroweak coupling constant α. The input masses and widths of the relevant particles which are used in the assignment of complex masses are

$$G_\mu = 1.16639 \times 10^{-5}\,\text{GeV}^{-2},$$
$$m_Z = 91.154\,\text{GeV}, \quad \Gamma_Z = 2.4956\,\text{GeV}$$
$$m_W = 80.358\,\text{GeV}, \quad \Gamma_W = 2.0890\,\text{GeV},$$
$$m_t = 173.34\,\text{GeV}, \quad \Gamma_t = 1.36918\,\text{GeV}. \tag{11}$$

The two parity-odd coefficients A_3 and A_4 show high sensitivity to the value of the weak mixing angle θ_W [14]. This is remedied by including the one-loop correction to the ρ-parameter in the LO and the NLO QCD predictions. Using the complex masses for the particles, this gives the effective value of

$$\sin^2 \theta_W = 1 - \left(\frac{\mu_W}{\mu_Z}\right)^2 + \Delta\rho \left(\frac{\mu_W}{\mu_Z}\right)^2, \tag{12}$$
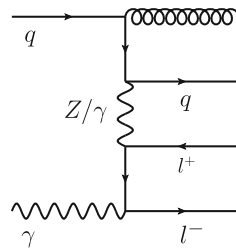
with the one-loop correction included from Ref. [25]

$$\Delta\rho = \frac{\sqrt{2}\bar{G}_\mu}{16\pi^2} 3\mu_t^2, \tag{13}$$

and applied with the complex-valued $\bar{G}_\mu$. The μ_Z, μ_W and μ_t are the complex masses for the Z- and W-bosons and the top quark, respectively. In the NLO EW predictions, these loop effects are already included as part of the loop corrections in the electroweak sector. The inclusion of the $\Delta\rho$ correction at

---

[1] The process where the recoil is a heavy vector boson is omitted from this work, albeit being of the order of interest. See Ref. [22] for discussion of the angular coefficients in such cases.

Fig. 1 An illustrative Feynman diagram from the photon induced real emission electroweak corrections leading to a double singularity uncanceled by virtual diagrams at the same order

this order in the electroweak corrections is redundant: a consistent inclusion of it is present in the loop diagrams. However, for a more elaborate and comprehensive treatment of the input parameters, one may employ the effective $\sin^2 \theta^l_{eff}$ scheme [26], in which a different set of input parameters are used than to the usual G_μ scheme, and the subtraction of the double counting in the electroweak correction is performed. For the purpose of the present work, our inclusion of the electroweak effects in the electroweak mixing angle is consistent and sufficient.

Photon recombination is performed with all light charged fermions on equal footing. A fermion (lepton or quark) is recombined with a photon if the distance in the $\eta - \phi$ plane, $R = \sqrt{\Delta\eta^2 + \Delta\phi^2}$, fulfills $R < 0.1$. Upon recombination, the photon momentum is added to the fermion momentum, and the former is removed from the list of external particles.

After recombination, the following basic cuts for event selection are applied. We use the narrow cut on the invariant mass of the lepton pair, the same as is used in the ATLAS measurement: $m_{ll} \in [80, 100]$ GeV. This we do in order for the Z-boson diagrams to be the dominant contribution, allowing for a determination of also the parity-odd coefficients A_3 and A_4. Events with lepton pair transverse momentum $p_{T,Z} > 11.4$ GeV are selected and results presented in the $p_{T,Z}$ range of [11.4, 400] GeV. We use no cuts on the jet transverse momentum and demand no reconstructed jet in the final state.

The soft and collinear divergences in the real-emission phase-space integration are canceled with the virtual corrections according to the Kinoshita–Lee–Nauenberg theorem [27,28]. For (N)NLO corrections in QCD, the requirement of non-zero p_T for the lepton pair (together with their invariant mass cut) is enough to render the process finite. However, when EW corrections are involved these cuts are not enough: in the photon induced, real emission diagrams, of which an illustrative example can be seen in Fig. 1, there can be double soft/collinear divergences. In the example diagram, the internal quark and lepton propagators can go on-shell simultaneously if the gluon and the electron are both collinear to the incoming partons. Such a double singularity is not canceled with a loop diagram at this order. In order to avoid these divergences, we place an additional single lepton transverse momentum cut (on both the negatively and positively charged leptons) for obtaining the differential distributions. This cut alters the setup of the ATLAS and CMS measurements, which

are performed inclusively in the lepton transverse momentum. Moreover, as this cut no longer allows for a full phase space inclusion of the final state leptons, the orthogonality relation, Eq. (5), which we use to compute the angular coefficients is, strictly speaking, no longer valid. To examine to which extent this cut affects the result, we present the differential distributions for three different values of the lepton transverse momentum cut: for $p_{T,l} > \{2.0, 5.0, 8.0\}$ GeV. Thus, we do not expect to be able to directly compare our predictions to data (which we therefore also do not show), but we should be able to address the size of the NLO EW corrections, at least in a qualitative manner, since both the LO and the NLO predictions will be affected by the cut.

The double singularity appearing in the real emission diagrams can be avoided by introducing the finite masses of the leptons. While this approach would avoid the singularities, the small masses of the electrons would yield logarithmically enhanced contributions, arising from a large difference between the scale and the mass. In order to avoid this issue, in this work we implement the technical transverse momentum cut on the single lepton and see to which extent this affects the final result.

3.2 Scale and PDF

For the scale choice, we follow Ref. [10] for the central value and the variation. We perform an uncorrelated variation of the renormalization and factorization scales in the numerator and denominator in Eq. (6) of the angular coefficients. Note that also the coefficient A_0 needs to be brought to a single quotient expression in order to apply this uncorrelated scale variation. For the choice of the central value, the transverse energy of the lepton pair is used,

$$\mu_0 = \sqrt{m_{ll}^2 + p_{T,Z}^2}. \tag{14}$$

Independently, we perform a 9-point scale variation for the numerator and denominator in each case, varying between $\frac{1}{2} \leq \mu_{\mathrm{R,F}}^{\mathrm{num,den}}/\mu_0 \leq 2$, and combining them in a way that $\frac{1}{2} \leq \mu_{\mathrm{R,F}}^{\mathrm{num}}/\mu_{\mathrm{R,F}}^{\mathrm{den}} \leq 2$ holds. The envelope is taken to be among these 31 possible combinations. The statistical error of the ratios is calculated by the usual propagation of errors.

For the numerical calculations, we use the PDF set LUXQED17_PLUS_PDF4LHC15_NNLO_100 [29] from the LHAPDF6 library [30], including the photon content in a more robust way, at all orders of the calculation. A comparison to results obtained with the NNPDF2.3 set [31] has been made, which is a set with a larger photon luminosity (and with much larger uncertainties), but the difference in the central values is negligible for the observables we consider in the following. The PDF uncertainties enter in the same manner in the numerator and denominator of Eq. (6), thus canceling

their effects in the angular coefficients to a large extent. This is the reason that they are omitted in this work.

4 Results

In Figs. 2, 3 and 4, we present the angular coefficients differentially as a function of the lepton pair p_T, following the setup as described in Sect. 3. The layout of all figures is identical. The same angular coefficient is shown in the left and right plots. In the main panel in the left plots, the LO (dotted) and NLO QCD (solid) predictions are shown, for the four values of the single lepton p_T cuts. In particular, the black, green, blue and red curves correspond to no p_T cut, $p_T > 2.0$ GeV, $p_T > 5.0$ GeV, and $p_T > 8.0$ GeV, respectively. In the middle panel, the ratio between the NLO QCD results, over the LO results are shown, and in the lower panel the uncertainties from scale variation are displayed for the NLO QCD result. In the figures on the right, the main panel shows the NLO QCD + EW predictions, now for three values of the single lepton transverse momentum.[2] The middle panel shows the ratio of the NLO QCD + EW predictions over the NLO QCD ones, and the lower panel displays the scale uncertainties at the NLO QCD + EW level. The only exception to this layout is in the two plots for the $A_0 - A_2$ (lower plots of Fig. 4) where in the middle insets the difference between the orders is taken, rather than their ratio. For all the coefficients shown here, the LO and NLO QCD predictions (without the single lepton p_T cut) are in agreement with the corresponding results presented in Ref. [10]. The results were checked against distributions obtained for the photon recombination parameter $R < 0.4$ instead of $R < 0.1$, and the difference in the final results is negligibly small for all observables considered here.

In the top two plots of Fig. 2 the A_0 coefficient is shown as a function of the transverse momentum of the lepton pair. From the main panels it is clear that the results, at LO, NLO QCD and NLO QCD + EW depend significantly on the size of the single lepton p_T cut. With the cut, the dependence of the coefficient on the lepton pair transverse momentum is reduced, resulting in a much flatter distribution. However, as can be seen from the middle panels, the ratios of the NLO QCD results over the LO ones (left plot) and the NLO QCD + EW over the NLO QCD ones (right plot), the NLO corrections are almost completely independent of the single lepton p_T cut, apart from the region $p_{T,Z} \lesssim 30$ GeV for the NLO EW corrections. In the latter region, the size of the NLO correction depends on the single lepton cut, with the smaller the cut, the larger the NLO correction. This is expected, since this contribution would be perturbatively unstable when letting

the value of the cut go to zero. For the region $p_{T,Z} \gtrsim 30$ GeV, the overall size of the corrections is small – both at the NLO QCD and NLO QCD + EW level it does not reach more than a couple of percent. In particular for the size of the EW corrections this is reassuring: since the dependence on the single lepton p_T cut is negligibly small, one can assume that the higher order EW effects are also negligible for the predictions without the single lepton p_T cut. Since the (N)NLO QCD predictions are in good agreement with the data for this observable [10], this remains true with the EW corrections included as well. The lower inset shows the scale uncertainties of the NLO QCD (left plot) and NLO QCD + EW (right plot) predictions. Since the EW corrections are small for this observable, also the two scale uncertainty bands are of very similar size, which is about $\pm 10\%$ at small and large $p_{T,Z}$ and a couple of percent points smaller for intermediate $p_{T,Z}$ values.

The A_2 coefficient is plotted in the lower two figures of Fig. 2. Similarly to the A_0 coefficient, also for this coefficient the single lepton transverse momentum cut flattens the value of the coefficient as a function of the lepton pair transverse momentum, albeit not in the same way. For this coefficient, the effect of the cut is much more pronounced at large values of $p_{T,Z}$, reducing the predictions for this coefficient by up to 50% at $p_{T,Z} \approx 300$ GeV. Interestingly, from the two middle panels one can conclude that the NLO (QCD and QCD + EW) corrections to this coefficient are almost completely insensitive to the single lepton transverse momentum cut. Hence, we can safely assume that the relative contributions from the EW corrections for the inclusive predictions would be similar in size as to what is given in the middle inset of the right plot. Indeed, from this middle panel we can see that the EW corrections are negligibly small for $p_{T,Z} \gtrsim 30$ GeV, but increase significantly below this value. In particular, they increase the NLO QCD results by more than a factor two for the smallest $p_{T,Z}$ values shown here. Comparing these corrections to the NNLO predictions from Ref. [10], we conclude that the NLO EW corrections are significantly larger than NNLO, and might overshoot in the comparison to the data in the first bin somewhat. The size of the uncertainties estimated from scale variations is similar for the NLO QCD and NLO QCD + EW predictions.

In the top two plots of Fig. 3 the A_1 coefficient is presented. As can be seen from the main and middle panels in the left figure, the NLO QCD corrections enhance the coefficient by up to 30% at the smallest Z-boson transverse momenta probed, but falling down to close to zero corrections at the largest transverse momenta ($p_{T,Z} \gtrsim 200$ GeV). These corrections are almost completely independent from the value of the single lepton p_T cut. On the other hand, the NLO QCD + EW corrections (as compared to the NLO QCD corrections alone) are completely flat in this observable, see the top and middle panels of the figure on the right hand side. Also these

---

[2] The inclusive results, i.e. without the single lepton p_T cut, are not IR-finite, as discussed in Sect. 2, and are therefore not shown.
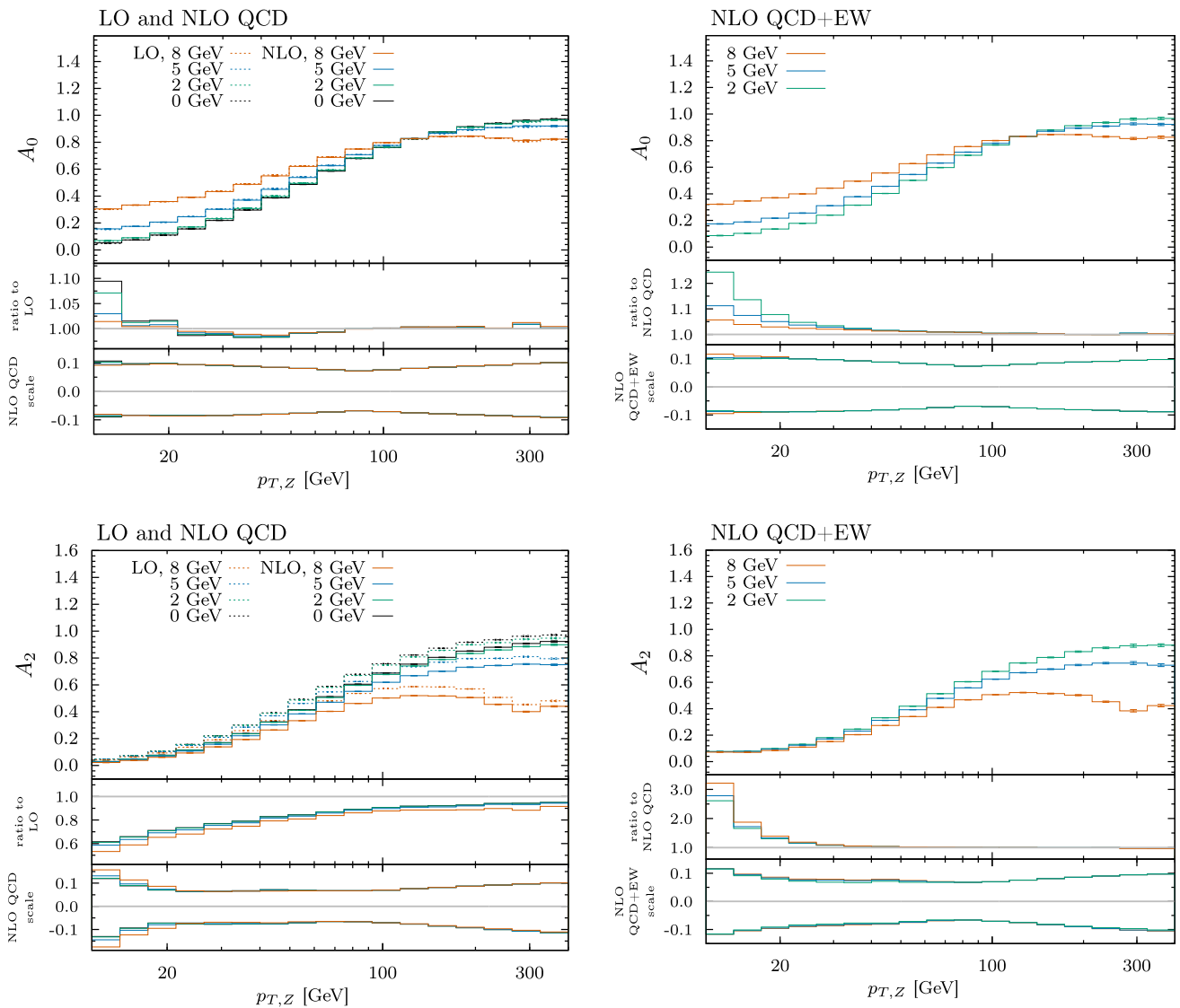
Fig. 2 The two largest angular coefficients A_0 (top) and A_2 (bottom), the LO and NLO QCD (left) and the NLO QCD + EW contribution (right) with corresponding ratios and scale uncertainties. The four (left) and three (right) different curves indicate the result with different values of the single lepton p_T cut. See text for more details

corrections are independent from the single lepton p_T cut, and it can therefore be assumed that the findings here can be extrapolated to the inclusive region. Since the EW corrections are small, the uncertainty from scale variations (lowest panels in both plots) is not affected to a significant extent by them.

The A_3 coefficient is shown in the lowest two figures of Fig. 3. The QCD corrections are small ($\lesssim 10\%$) and almost independent from the single lepton p_T cut, as can be seen from the top and middle panels of the left plot. The NLO EW corrections on top of the NLO QCD ones are of order of ten percent throughout the $p_{T,Z}$ interval, and also here independent of the single lepton cut. Similarly to the other

coefficients, the relative uncertainties from scale variation is similar for the NLO QCD and NLO QCD + EW predictions (see the bottom panels of both plots). We remind the reader that in our LO and NLO QCD predictions we include the dominant EW corrections to the ρ parameter, see Sect. 3. Having included it, the EW correction on top of the QCD correction is somewhat reduced to roughly -10%. We note however that this is an overall, transverse momentum independent shift, one which is also present in the A_4 coefficient (see upper figures in Fig. 4). As these coefficients are the most sensitive to the weak mixing angle, this overall shift may be a consequence of missing higher order corrections in this parameter. More precisely, the two-loop contribution to
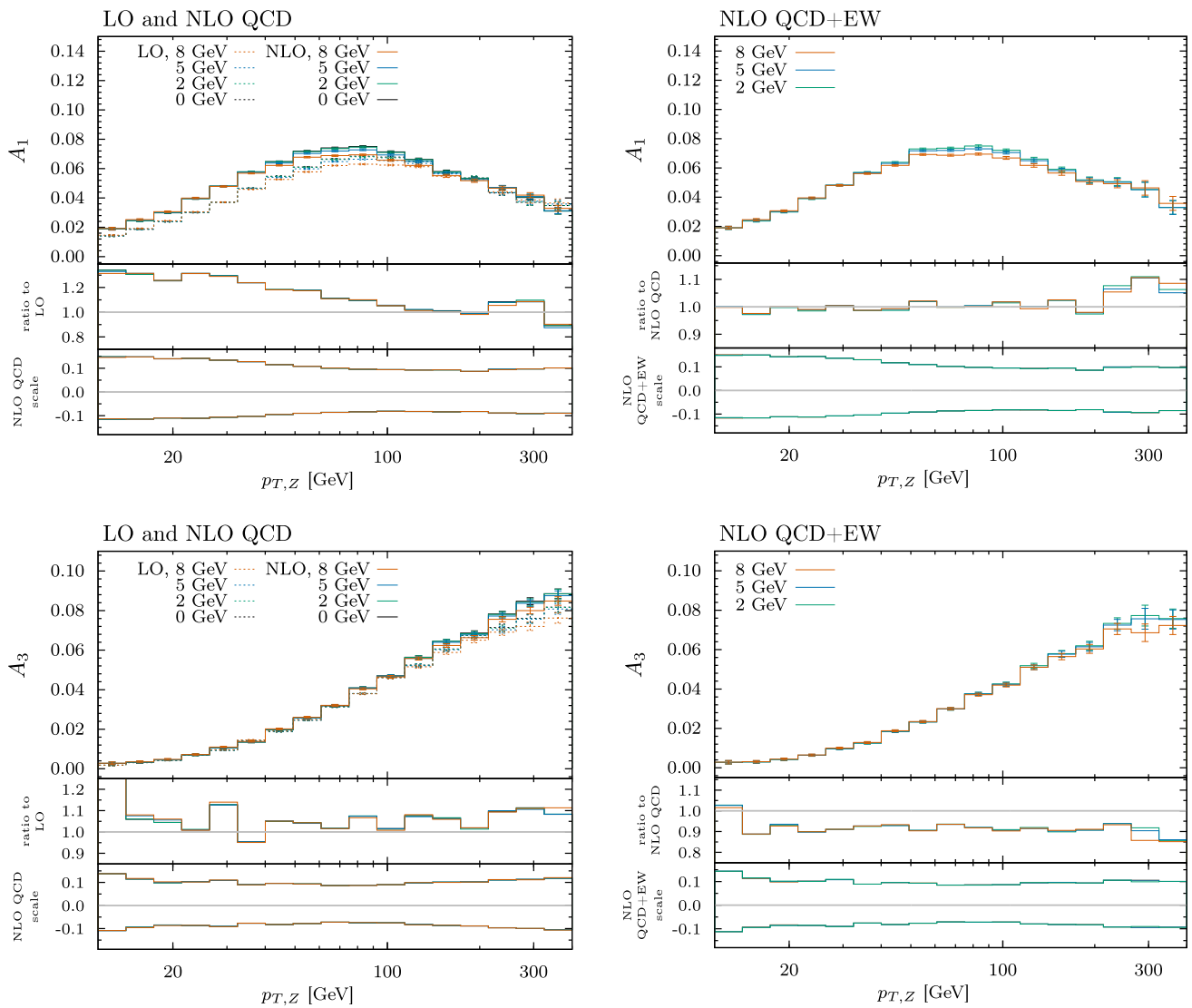
Fig. 3 The two angular coefficients A_1 (top) and A_3 (bottom), the LO and NLO QCD (left) and the NLO QCD + EW contribution (right) with corresponding ratios and scale uncertainties. The four (left) and three (right) different curves indicate the result with different values of the single lepton p_T cut. See text for more details

the ρ-parameter in Eq. 13 may mitigate this overall shift in these coefficients. As such, these overall large electroweak corrections to these coefficients are not an artifact of the perturbative behavior.

The predictions for the A_4 coefficient is shown in the top two plots of Fig. 4. As can be seen from the top panels in both figures, the predictions for this coefficient are rather independent from the value of the single lepton transverse momentum cut. Moreover, also the NLO QCD and EW corrections are independent from this cut, as can be seen from the two middle panels. The size of the NLO QCD corrections (of about a few percent) is somewhat smaller than the EW corrections on top of the QCD corrections. Since this correction is independent from the single lepton p_T cut this can be extrapolated

to the inclusive result. We point out once more the issue with the sensitivity on the weak mixing angle of this coefficient, as in the case of the A_3 coefficient, yielding the large order ten percent EW correction. Would we not have included the one-loop corrections to the ρ-parameter, the NLO EW corrections to this coefficient would have resulted in a very large of about -30% correction over the whole $p_{T,Z}$ range The uncertainty band is not altered significantly after including EW corrections, which can be seen in the lower panel.

In the bottom two plots of Fig. 4 we show the predictions for the violation of the Lam–Tung relation, i.e. the left hand side of Eq. (4). As expected, see Fig. 2, the dependence on the single lepton transverse momentum cut is significant for the violation. However, the actual size of the NLO correc-
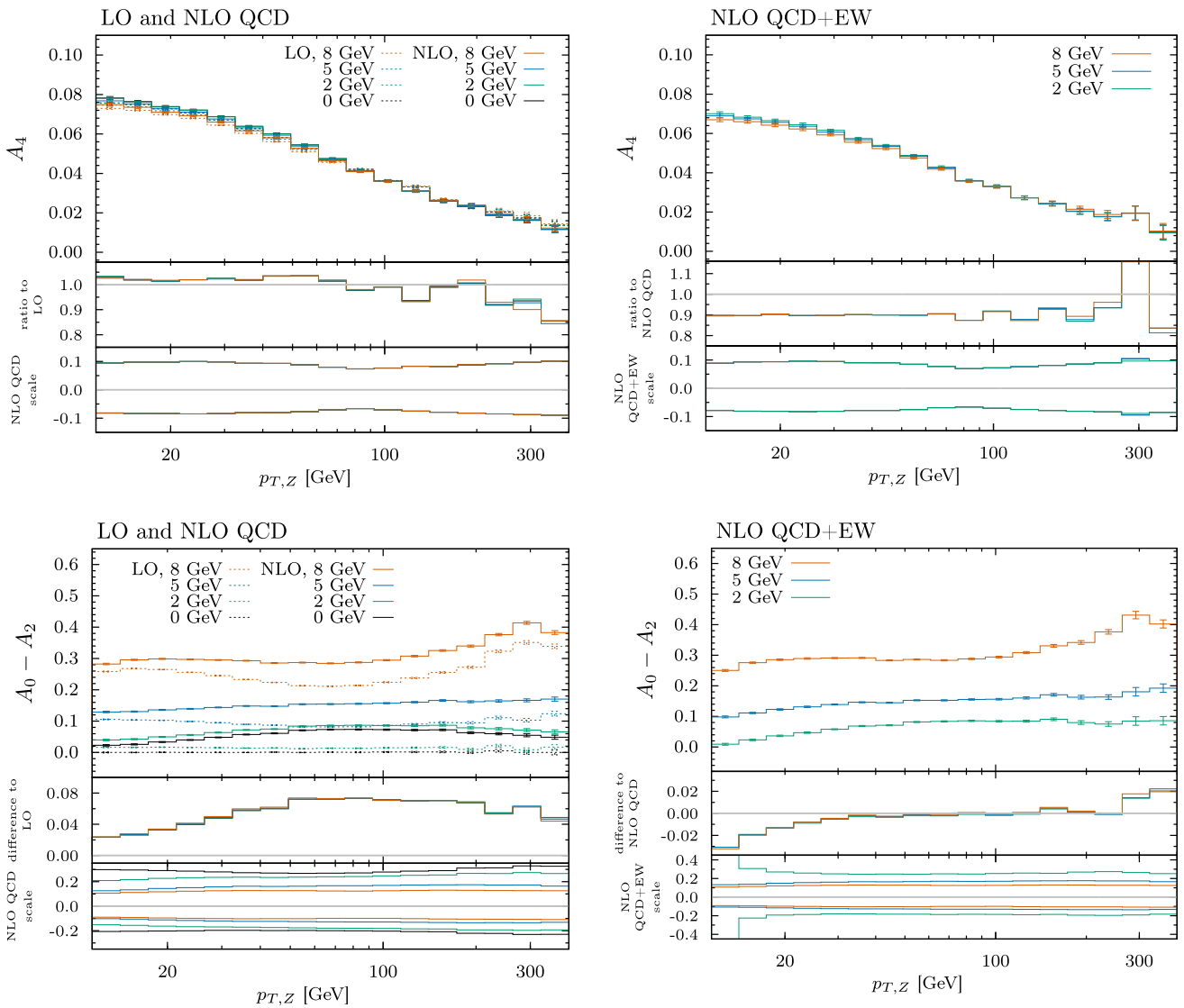
Fig. 4 The angular coefficient A_4 (top) and the Lam–Tung difference $A_0 - A_2$ (bottom), the LO and NLO QCD (left) and the NLO QCD + EW contribution (right) with corresponding ratios and scale uncertainties. The four (left) and three (right) different curves indicate the result with different values of the single lepton p_T cut. See text for more details

tions (both QCD and EW), is rather independent from this cut, as can be seen from the two middle panels.[3] From the middle inset of the right hand figure, we can conclude that the NLO EW corrections change the violation of the Lam–Tung relation by up to -0.03 at the smallest $p_{T,Z}$ considered, but reducing with increasing $p_{T,Z}$ and already compatible with zero at $p_{T,Z} \approx 25$ GeV. A correction of -0.03 is rather significant, since the complete NNLO predictions in this p_T range are around 0.05 or below [10] when not imposing the single lepton p_T cut.

5 Conclusions and discussions

In this paper we have examined the five dominant angular coefficients parametrizing the cross section of Z-boson production at finite-p_T and decay to the leptonic final state l^+l^- at $\mathcal{O}(\alpha^3 \alpha_S)$ at pp collisions at $\sqrt{s} = 8$ TeV. We have presented the results differentially in the lepton pair transverse momentum $p_{T,Z}$. We compared our NLO QCD + EW results to the NLO QCD predictions, in the invariant mass range $m_{ll} \in [80, 100]$ GeV. We examined the effect of a single lepton transverse momentum cut, which is included to avoid IR singularities in the electroweak corrections.

For the variation of the single lepton p_T cut, the general feature we find is that the coefficients depend on the cut in

---

[3] We remind the reader that these middle insets is not a ratio, but rather the difference between the NLO QCD and LO predictions (left plot) and NLO QCD + EW and NLO QCD ones (right plot).

a similar manner at all orders of interest: A_1, A_3 and A_4 are found to be the least affected by the value of the cut at LO, NLO QCD and NLO QCD + EW, whereas A_0 and A_2 show a rather significant dependence on this cut in certain regions. The relative sizes of the dependencies manifest themselves in the level of the Lam–Tung violation, for which we find an increasing violation for an increasing single lepton cut, as expected. On the other hand, by examining the ratios of NLO QCD/LO and NLO QCD + EW/QCD it can be concluded that most of the dependence on the single lepton p_T cut factors from the corrections: the dependence on the cut is similar for the LO, NLO QCD and NLO QCD + EW predictions. The only minor exception to this can be found for the low-p_T bins of the A_0 coefficient, where an increase in the cut decreases the significance of the EW corrections (which is compatible with what can be expected from perturbation theory). Even though this effect is significant for this coefficient, this does not affect the Lam–Tung violation, where there is again only a negligible dependence on the single lepton cut in the size of the NLO QCD and NLO QCD + EW corrections.

The fact that the relative dependence on the single lepton p_T cut is almost always negligible for the corrections, allows us to make the following conclusions about the importance of the fixed-order EW corrections. For the A_0 coefficient the EW corrections are negligible, except in the region $p_{T,Z} \lesssim 30$ GeV, for which these predictions cannot be trusted. Similarly, for the A_2 coefficient the EW corrections are small, except in the region $p_{T,Z} \lesssim 30$ GeV, where they rise steeply, resulting in corrections of more than a factor two on top of the NLO QCD ones. For the A_1 coefficient, the EW corrections are negligible. For the two remaining coefficients A_3 and A_4, which are sensitive to the weak mixing angle, with our inputs to the calculation, we find a large ten percent EW correction. This, however, is an overall shift, and a even more fine-tuning of this parameter may reduce the size of these corrections. For the violation of the Lam–Tung relation, the NLO QCD + EW corrections are marginal compared to the NLO QCD corrections for $p_{T,Z} \gtrsim 25$ GeV. However, for $p_{T,Z} \lesssim 25$ GeV the EW corrections increase, resulting in a rather significant -0.03 correction to the Lam–Tung violation at the smallest $p_{T,Z}$ values considered.

Data Availability Statement This manuscript has no associated data or the data will not be deposited. [Authors' comment: The theoretical data is presented as tables in the article, while no experimental data is to be presented.]

References

1. J.C. Peng, J.W. Qiu, Prog. Part. Nucl. Phys. **76**, 43 (2014). https://doi.org/10.1016/j.ppnp.2014.01.005
2. S. Drell, T.M. Yan, Phys. Rev. Lett. **25**, 316 (1970). https://doi.org/10.1103/PhysRevLett.25.316. [Erratum: Phys. Rev. Lett. 25, 902 (1970)]
3. G. Altarelli, R. Ellis, G. Martinelli, Nucl. Phys. B **143**, 521 (1978). https://doi.org/10.1016/0550-3213(78)90067-6. [Erratum: Nucl. Phys. B 146, 544 (1978)]
4. J.C. Collins, D.E. Soper, Phys. Rev. D **16**, 2219 (1977). https://doi.org/10.1103/PhysRevD.16.2219
5. C. Lam, W.K. Tung, Phys. Rev. D **18**, 2447 (1978). https://doi.org/10.1103/PhysRevD.18.2447
6. C. Lam, W.K. Tung, Phys. Rev. D **21**, 2712 (1980). https://doi.org/10.1103/PhysRevD.21.2712
7. J. Callan, G. Curtis, D.J. Gross, Phys. Rev. Lett. **22**, 156 (1969). https://doi.org/10.1103/PhysRevLett.22.156
8. M. Chaichian, M. Hayashi, K. Yamagishi, Phys. Rev. D **25**, 130 (1982). https://doi.org/10.1103/PhysRevD.25.130. [Erratum: Phys. Rev. D 26, 2534 (1982)]
9. E. Mirkes, J. Ohnemus, Phys. Rev. D **51**, 4891 (1995). https://doi.org/10.1103/PhysRevD.51.4891
10. R. Gauld, A. Gehrmann-De Ridder, T. Gehrmann, E. Glover, A. Huss, JHEP **11**, 003 (2017). https://doi.org/10.1007/JHEP11(2017)003
11. T.A. Aaltonen et al., Phys. Lett. B **692**, 232 (2010). https://doi.org/10.1016/j.physletb.2010.06.043
12. V. Abazov et al., Phys. Rev. D **76**, 012003 (2007). https://doi.org/10.1103/PhysRevD.76.012003
13. V. Khachatryan et al., Phys. Lett. B **750**, 154 (2015). https://doi.org/10.1016/j.physletb.2015.08.061
14. G. Aad et al., JHEP **08**, 159 (2016). https://doi.org/10.1007/JHEP08(2016)159
15. J.C. Peng, W.C. Chang, R.E. McClellan, O. Teryaev, Phys. Lett. B **758**, 384 (2016). https://doi.org/10.1016/j.physletb.2016.05.035
16. A. Brandenburg, S. Brodsky, V.V. Khoze, D. Mueller, Phys. Rev. Lett. **73**, 939 (1994). https://doi.org/10.1103/PhysRevLett.73.939
17. D. Boer, Phys. Rev. D **60**, 014012 (1999). https://doi.org/10.1103/PhysRevD.60.014012
18. E. Mirkes, Nucl. Phys. B **387**, 3 (1992). https://doi.org/10.1016/0550-3213(92)90046-E
19. A. Denner, S. Dittmaier, T. Kasprzik, A. Muck, JHEP **06**, 069 (2011). https://doi.org/10.1007/JHEP06(2011)069
20. J. Alwall, R. Frederix, S. Frixione, V. Hirschi, F. Maltoni, O. Mattelaer, H.S. Shao, T. Stelzer, P. Torrielli, M. Zaro, JHEP **07**, 079 (2014). https://doi.org/10.1007/JHEP07(2014)079
21. R. Frederix, S. Frixione, V. Hirschi, D. Pagani, H.S. Shao, M. Zaro, JHEP **07**, 185 (2018). https://doi.org/10.1007/JHEP07(2018)185
22. J. Baglio, N. Le Duc, JHEP **04**, 065 (2019). https://doi.org/10.1007/JHEP04(2019)065
23. A. Denner, S. Dittmaier, M. Roth, D. Wackeroth, Nucl. Phys. B **560**, 33 (1999). https://doi.org/10.1016/S0550-3213(99)00437-X

24. A. Denner, S. Dittmaier, M. Roth, L. Wieders, Nucl. Phys. B **724**, 247 (2005). https://doi.org/10.1016/j.nuclphysb.2011.09.001. [Erratum: Nucl. Phys. B 854, 504-507 (2012)]

25. J. Fleischer, O. Tarasov, F. Jegerlehner, Phys. Lett. B **319**, 249 (1993). https://doi.org/10.1016/0370-2693(93)90810-5

26. M. Chiesa, F. Piccinini, A. Vicini, Phys. Rev. D **100**(7), 071302 (2019). https://doi.org/10.1103/PhysRevD.100.071302

27. T. Kinoshita, J. Math. Phys. **3**, 650 (1962). https://doi.org/10.1063/1.1724268

28. T. Lee, M. Nauenberg, Phys. Rev. **133**, B1549 (1964). https://doi.org/10.1103/PhysRev.133.B1549

29. A.V. Manohar, P. Nason, G.P. Salam, G. Zanderighi, JHEP **12**, 046 (2017). https://doi.org/10.1007/JHEP12(2017)046

30. A. Buckley, J. Ferrando, S. Lloyd, K. Nordström, B. Page, M. Rüfenacht, M. Schönherr, G. Watt, Eur. Phys. J. C **75**, 132 (2015). https://doi.org/10.1140/epjc/s10052-015-3318-8

31. R.D. Ball et al., Nucl. Phys. B **867**, 244 (2013). https://doi.org/10.1016/j.nuclphysb.2012.10.003